Crystallization and Transformation of Polymorphic Forms of trioleoyl glycerol (OOO) and 1,2-dioleoyl-3-*rac*-linoleoyl glycerol (OOL)

Laura Bayés-García,[*a] Teresa Calvet[a], Miquel Àngel Cuevas-Diarte[a], Satoru Ueno[b], and Kiyotaka Sato[b]*

[a]Departament de Cristal·lografia, Mineralogia i Dipòsits Minerals, Facultat de Geologia, Universitat de Barcelona, Martí i Franquès s/n, E-08028 Barcelona, Spain.

[b]Faculty of Applied Biological Science, Hiroshima University, Higashi-Hiroshima 739, Japan.

KEYWORDS. Polymorphism, Crystallization, Triacylglycerol, X-ray diffraction, DSC, Kinetic effects

ABSTRACT

This study examined the influence of different thermal treatments on the crystallization and transformation of trioleoyl glycerol (OOO) and 1,2-dioleoyl-3-*rac*-linoleoyl glycerol (OOL). Two triacylglycerol (TAG) samples were cooled at 0.5 to 15ºC·min^{-1} and heated at 2 and 15ºC·min^{-1}. The polymorphic characteristics of the two TAGs were analyzed *in-situ* using differential scanning calorimetry (DSC), Raman spectroscopy, and synchrotron radiation X-ray diffraction (SR-XRD). Multiple polymorphic forms were identified in OOO (α, β'_2, β'_1, β_2, and β_1) and OOL (α, β'_2, and β'_1). Larger quantities of more stable forms (e.g., β_2 and β_1 of OOO, and β'_1 of OOL) were obtained when the samples were slowly cooled and heated. In contrast, less stable polymorphs were obtained with increased cooling and heating rates. Polymorphic transformations occurred in either solid-state or melt-mediation and were influenced by heating rates.

The results were analyzed by considering the activation energies for crystallization and transformation of stable and less stable polymorphic forms in comparison with previous studies on 1, 3-dipalmitoyl-2-oleoyl-glycerol (POP) and 1, 3-dioleoyl-2-palmitoyl-glycerol (OPO).

INTRODUCTION

Lipids are major nutrients employed in the food, pharmaceutical, and cosmetic industries[1] as lipophilic materials. In this large group of compounds, triacylglycerols (TAGs) are the main components of natural and industrial fats and oils. The physical properties (e.g., melting, morphology, rheology, and texture[2]) of TAGs depend mainly on their fatty acid structures and compositions, which are most typically revealed in polymorphism. The complexity of polymorphism and the number of polymorphic forms of TAGs are strongly related to the chemical nature of the fatty acid components (chain length, saturated or unsaturated, *cis* or *trans* double bonds).[1]

Controlling the polymorphism of TAGs to obtain the desired product characteristics is an important challenge for the industrial fields (e.g., pharmaceutical, biomedical, and food). Therefore, many studies have addressed the influence of external factors on the polymorphic characteristics of TAGs (e.g., additives,[3] shear,[4] and sonication[5]).

The effects of temperature variation have also been studied, since the kinetic properties of polymorphic crystallization and transformation of TAGs are significantly influenced by the rates of cooling and heating of the TAG samples in neat liquid and emulsion states. This is because the influences of dynamic temperature variations are exhibited differently in metastable forms than in more stable polymorphic forms. Thus, many researchers have studied the influences of thermal treatments on the polymorphic behavior of TAGs, from pure TAGs[6-8] to more complex or natural samples.[9-12] Recently, we reported on the effects of varied cooling rates on the polymorphic crystallization of 1,3-dioleoyl-2-palmitoyl glycerol (OPO),[7] and the effects of changing both cooling and heating rates on the crystallization and transformation pathways of 1,3-dipalmitoyl-

2-oleoyl glycerol (POP)[8] using differential scanning calorimetry (DSC) and synchrotron radiation X-ray diffraction (SR-XRD) with small-angle X-ray diffraction (SAXD) and wide angle X-ray diffraction (WAXD). SR-XRD and DSC provided highly accurate information and permitted *in-situ* monitoring of the polymorphic crystallization and subsequent transformations, even if high cooling/heating rates (e.g., 15ºC·min^{-1}) were applied.

This study reports on the polymorphic characteristics of trioleoyl-glycerol (OOO) and 1,2-dioleoyl-3-linoleoyl glycerol (OOL), which are the main triunsaturated TAGs present in vegetable oils (e.g., olive oil[13]) and other edible oils, by dry fractionation of palm oil.[14] The crystallization characteristics of these low-melting TAGs are important for the physical properties of foods employed at chilled temperatures (e.g., frozen foods).

Regarding the polymorphism of OOO, Wheeler et al.[15] demonstrated the existence of "three crystalline or solid forms: Form I, Form II, and Form III" and presented their melting point data. Later, Ferguson et al.[16] determined the long- and short-spacing values of three polymorphic forms of OOO: α, β', and β. More polymorphs were characterized by Hagemann et al.,[17] who reported that three β' forms (β'$_1$, β'$_2$, and β'$_3$) appeared when different thermal treatments were applied. They conducted DSC and IR experiments but provided no XRD data on the newly found β' forms. Sato and Ueno noted the presence of three β' forms and two β forms in OOO[18] but presented no details. Akita et al.[19] recently reported the molecular conformations and crystal structures of α, β', and β forms using a combination of XRD, infra-red (IR), and Raman methods. However, few studies have focused on the kinetic properties of the crystallization and transformation of polymorphic forms of OOO.

In this study, we applied DSC, SR-XRD, and micro-Raman methods to *in-situ* observation of the crystallization and transformation kinetics of OOO and OOL. In order to avoid the effects of impurities on polymorphic characteristics, we used highly pure samples of OOO and OOL. Different thermal treatments were applied to the samples by changing the cooling and heating rates. Long- and short-spacing values were determined for all the studied polymorphic forms of OOO (α, β'_2, β'_1, β_2, and β_1) and OOL (α, β'_2, and β'_1). To the best of our knowledge, this study is the first to examine the polymorphic characteristics of OOL.

MATERIALS AND METHODS

Samples of OOO and OOL were purchased from Tsukishima Foods Industry Co., Ltd. (Tokyo, Japan) and used without further purification. The sample purity was 99.4% (OOO) and 99.0% (OOL), analyzed using HPLC (private communication from Tsukishima Foods Industry Co., Ltd.).

DSC experiments were conducted at atmospheric pressure using both a Perkin-Elmer DSC-7 (for the shortest thermal treatments) and a Perkin-Elmer DSC Diamond (for the longest ones). The DSC thermograms obtained by the two calorimeters were comparable. Samples (9.0 to 9.4mg) were weighted into 50µl aluminium pans, and covers were sealed into place. Both instruments were calibrated with reference to the enthalpy and the melting points of indium (melting temperature: 156.6ºC; ΔH: 28.45J/g) and decane (melting temperature: -29.7ºC; ΔH: 202.1J/g) standards. An empty pan was used as a reference. Dry nitrogen was used as purge gas in the DSC cell (at 23cm^3/min in the Perkin-Elmer DSC-7 and at 20cm^3/min in the Perkin-Elmer DSC Diamond). Thermograms were analyzed with Pyris Software to obtain the enthalpy (J/g,

integration of the DSC signals) and T_{onset} of the transitions (ºC, intersections of the baseline and the initial tangent at the transition).

Samples were subjected to different cooling and heating rates in the following patterns. OOO was cooled (15, 2, 1, and 0.5ºC·min^{-1}), heated (15ºC·min^{-1}), cooled (2ºC·min^{-1}) and heated (2ºC·min^{-1}). OOL was cooled (15ºC·min^{-1}), heated (15 and 0.5ºC·min^{-1}), cooled (2ºC·min^{-1}), heated (2ºC·min^{-1}), cooled (0.5ºC·min^{-1}), and heated (15ºC·min^{-1}). At least three independent measurements were made for each experiment (n = 3). Random uncertainty was estimated with a 95% threshold of reliability using the Student's t-distribution, which enables estimation of the mean of a normally distributed population when it is small.[20] A correction (described elsewhere[7]) was applied for analyses with cooling or heating rates other than 2ºC·min^{-1}, since both calorimeters were calibrated at this rate.

SR-XRD experiments were performed at two different beamlines (BL-15A and BL-9C) of the SR source Photon Factory (PF) of the High-Energy Accelerator Research Organization (KEK) in Tsukuba (Japan). For both beamlines, a double-focusing camera operated at a wavelength of 0.15nm. In BL-9C, the X-ray scattering data were simultaneously collected by Position Sensitive Proportional Counters (PSPCs) (Rigaku Co., PSPC-10) SAXD and WAXD. In BL-15A, a camera with a charge-coupled device (CCD) was used for small-angle data, and a PSPC for wide-angle data. Each temperature program was controlled by a Mettler DSC-FP84 (Mettler Instrument Corp., Greifensee, Switzerland) with FP99 software. A 2mm-thick sample was placed in an aluminium sample cell with Kapton film windows. SR-XRD spectra were acquired at 30 or 60s intervals, depending on the cooling and heating rates used and the complexity of the thermal profile.

Conventional powder XRD was used for some intermediate cooling and heating rates using a PANalytical X'Pert Pro MPD powder diffractometer equipped with a Hybrid Monochromator and an X'Celerator Detector. The equipment also included an Oxford Cryostream Plus 220V (temperature 80 to 500K). This diffractometer operates with Debye-Scherrer transmission. The sample was introduced in a 1mm-diameter Lindemann glass capillary that was rotated around its axis during the experiment to minimize preferential orientation of the crystallites. The step size was 0.013º from 1.004º to 28º 2θ and the measuring time was 2.5min per pattern.

Micro-Raman spectra were measured with a dispersive Jobin-Yvon Lab Ram HR 800 spectrometer, with a 532nm line as the excitation source. The laser power was 6mW at the sample point. The detector was a CCD, which was cooled at -70ºC. The spectrometer was coupled to an optic microscope Olympus BXFM (50x). A Linkam THMG600/720 stage, with a PE95/T95 temperature controller and an LNP liquid-nitrogen cooling system, was installed on the microscope. Samples were put on an aluminium sample cell in the Linkam stage. Raman spectra were obtained for an exposure time of 15s. The coupling of the Linkam stage and the micro-Raman equipment permitted us to follow thermal treatments closely, controlling the cooling and heating rates in a wide temperature range.

RESULTS AND DISCUSSION

General polymorphic properties

Table 1 summarizes the melting points and long/short-spacing values of the polymorphs of OOO and OOL examined in the present work.

Table 1. Long and short spacing values of the polymorphic forms of OOO and OOL. Unit, nm.

OOO			
	Melting temperature (°C)	Long spacing	Short Spacing
α-2	-33	4.5	0.431 with shoulder
β'_2-2	---	4.5	0.434, 0.405
β'_1-2	-13	4.5	0.452, 0.436, 0.407, 0.393
β_2-2	-2	4.4	0.458 (0.456), 0.448, 0.398, 0.389, 0.378
β_1-2	2.9	4.4	0.458 (0.456), 0.448, 0.435, 0.405, 0.399, 0.387, 0.381, 0.377, 0.374, 0.368
OOL			
	Melting temperature (°C)	Long Spacing	Short Spacing
α-2	-60	4.4	0.421 with shoulder
β'_2-2	-25	4.4	0.433, 0.410
β'_1-2	-21	4.5	0.453, 0.438, 0.391

Long-spacing values were used for determining the chain-length structures, whereas short-spacing values permitted us to identify the polymorphic forms. These polymorphic forms are defined according to their subcell structures which correspond to cross-sectional packing modes of the zigzag aliphatic chains[1]. Thus, in general, α form is defined by a hexagonal subcell (H), β' form has an orthorhombic perpendicular subcell ($O_\perp$), and the subcell of β form is triclinic parallel ($T_{//}$). The XRD data of three forms of OOO (α, β', and β) have been determined in previous studies[16, 19] whose data are in good agreement with those reported in the present study.

Additionally, we observed the long- and short-spacing values of two β' forms (β'_2 and β'_1) and two β forms (β_2 and β_1) of OOO. Previously, Hagemann et al.[17] confirmed the existence of three β' forms (β'_3, β'_2, and β'_1). Using IR, they could determine the typical orthorhombic subcell structure of β' form and the DSC data permitted to differentiate three β' forms; however, no XRD data were given. Akita et al.[19] reported only one form of β' and β, corresponding to β'_1 and β_1 of the present study in accordance with the melting points.

No β form was observed for OOL, since the short-spacing pattern of 0.458nm, which is typical of the triclinic subcell of β form, was not detectable. Instead, two β' forms were observed as the most stable polymorphs.

The chain-length structures of all the polymorphic forms of OOO and OOL are double (Table 1). From the long-spacing values observed, we can conclude that the inclination angles are relatively large even in the α phases. Compared with the long-spacing values of the corresponding trisaturated TAG (tristearin (SSS)), the difference in the long-spacing values between polymorphs of OOO and OOL is much smaller. SSS exhibits long spacing at 5.06, 4.72, and 4.50nm for the corresponding polymorphs (α, β', and β).[21] The large long-spacing value of α of SSS is due to the perpendicular orientation of the acyl chains against the lamellar surface, and the acyl chains are more inclined in the order of β' and β. Therefore, the smaller long-spacing value of α form for OOO and OOL than for SSS may indicate that the presence of *cis*-double bonds may shorten lamellar distance. The structure models of OOO and OOL will be discussed later.

Polymorphic characteristics of OOO

Figure 1 depicts the DSC thermograms of OOO taken by cooling from the melt at different rates (15ºC·min^{-1}, 2ºC·min^{-1}, 1ºC·min^{-1}, and 0.5ºC·min^{-1}) and heated at 15ºC·min^{-1}.

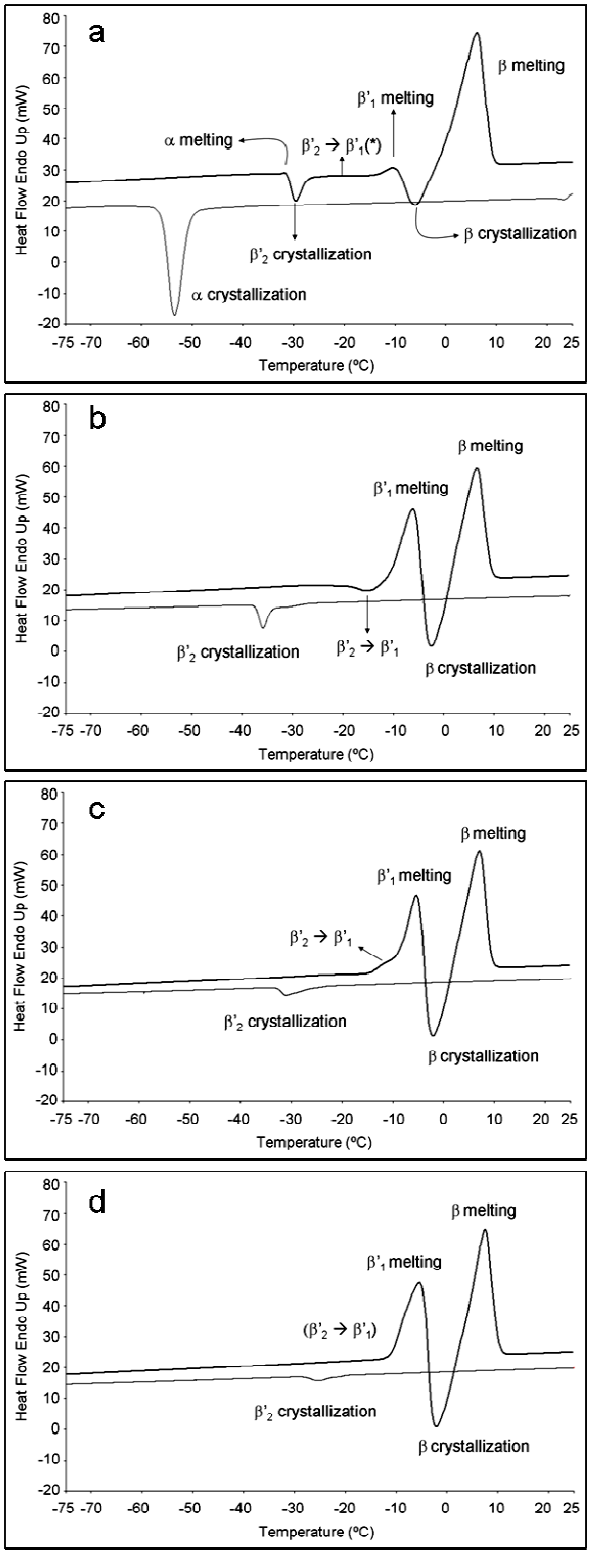

Figure 1. DSC thermograms of OOO obtained by applying different cooling rates (heating rate was always 15 ºC·min^{-1}). (a) 15ºC·min^{-1}, (b) 2ºC·min^{-1}, (c) 1ºC·min^{-1} and (d) 0.5ºC·min^{-1}.

The DSC data, including the onset temperature (T_{onset}) and enthalpy (ΔH) associated with each transition, are presented in Table 2.

Table 2. DSC data of the polymorphic crystallization and transformation of OOO obtained when the sample was cooled and heated at different rates. The letters *c*, *s* and *m* mean crystallization, solid-state transformation and melting, respectively.

	Cooling (15ºC·min^{-1})		**Heating (15ºC·min^{-1})**				
Polymorph	α *(c)*		α *(m)*	β'_2 *(c)*	β'_1 *(m)*	β *(c)*	β *(m)*
T (ºC)	-51.1 ± 0.6		-34.1 ± 0.5	-32.3 ± 0.5	-14.4 ± 0.5	-10.2 ± 0.8	-3.3 ± 0.8
ΔH (J/g)	-54 ± 2		aprox. 0	-9 ± <1	2 ± 1	-16 ± 2	105 ± 17
	Cooling (2ºC·min^{-1})		**Heating (15ºC·min^{-1})**				
Polymorph	β'_2 *(c)*		$\beta'_2 \rightarrow \beta'_1$	β'_1 *(m)*	β *(c)*	β *(m)*	
T (ºC)	-26.6 ± 1.2	-33.4 ± 0.7	-20.8 ± 1.3	-13.3 ± 0.6	-5.3 ± 0.4	0.4 ± 0.4	
ΔH (J/g)	-70 ± 1		-6 ± 3	41 ± 2	-33 ± 3	73 ± 3	
			(2º C·min^{-1})				
Polymorph			$\beta'_2 \rightarrow \beta_2$	$\beta_2 \rightarrow \beta_1$	$\beta_2 + \beta_1$ *(m)*		
T (ºC)			-25 ± 1.7	-11.3 ± 1.7	-2.2 ± 0.7	2.9 ± 1.3	
ΔH (J/g)			*	-27 ± 4	128 ± 5**		
	Cooling (1ºC·min^{-1})		**Heating (15ºC·min^{-1})**				
Polymorph	β'_2 *(c)*		$\beta'_2 \rightarrow \beta'_1$	β'_1 *(m)*	β *(c)*	β *(m)*	
T (ºC)	-22.3 ± 0.7	26.3 ± 3.1	-15.7 ± 0.8	-11.2 ± 0.4	-5.0 ± 0.6	0.6 ± 0.5	
ΔH (J/g)	-76 ± 3		40 ± 2**		-31 ± 2	71 ± 2	
	Cooling (0.5ºC·min^{-1})		**Heating (15ºC·min^{-1})**				
Polymorph	β'_2 *(c)*		β'_1 *(m)*	β *(c)*	β *(m)*		
T (ºC)	-19.1 ± 1.5	21.5 ± 0.7	-12.2 ± 1.2	-4.5 ± 1.1	1.3 ± 1		
ΔH (J/g)	-83 ± 5		45 ± 4	-33 ± 6	73 ± 8		

* It was not possible to determine this value, as the nature of this transformation pathway is not clear (see text).

** These enthalpy values correspond to the global enthalpy of overlapped peaks.

To identify the crystallization and transformation processes of the polymorphic forms exhibited in exothermic and endothermic DSC peaks, we conducted SR-XRD experiments by applying the same thermal treatments as DSC (Fig. 2).

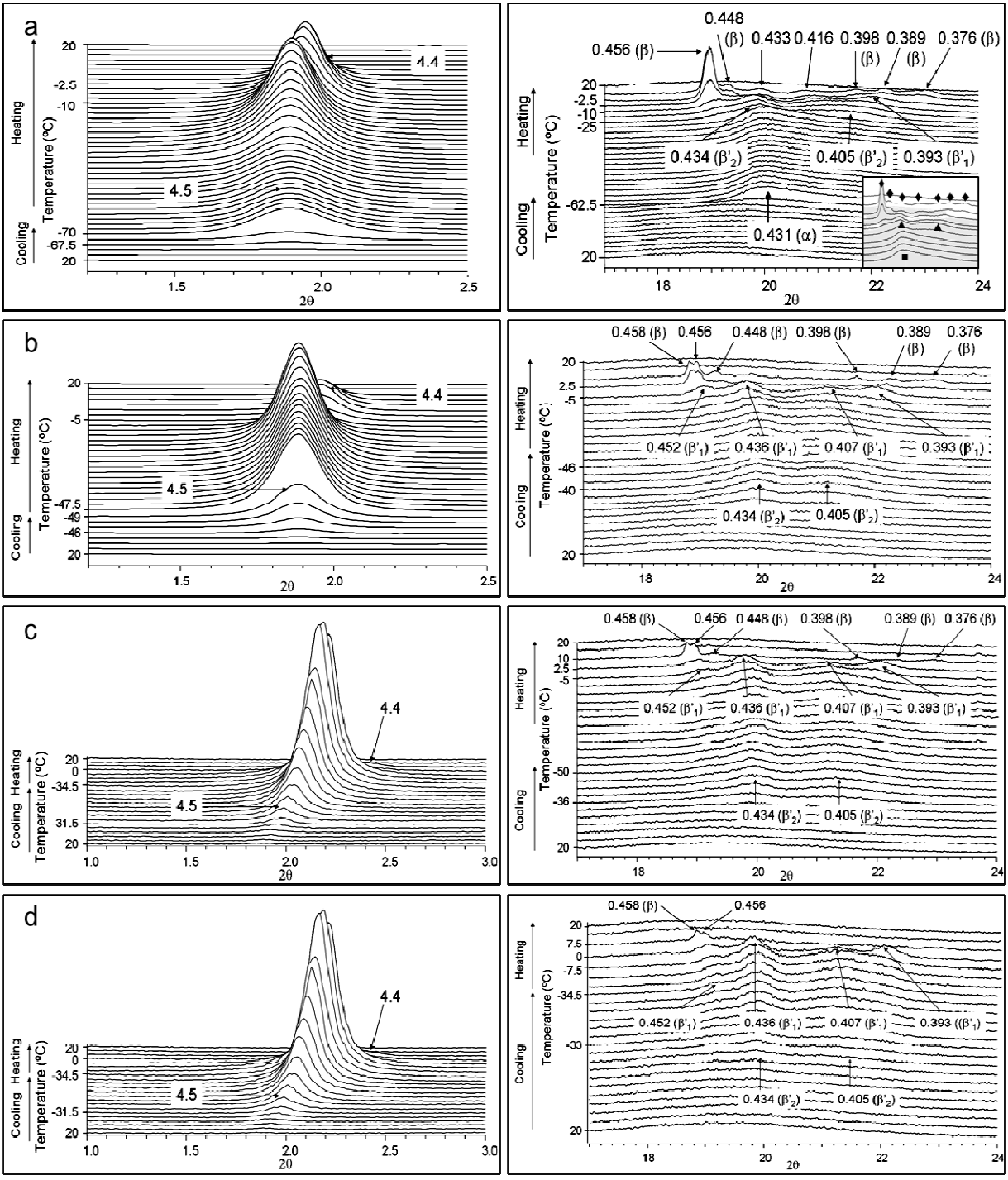

Figure 2. SR-XRD patterns of OOO obtained by applying different cooling rates (heating rate was always 15 ºC·min^{-1}). (a) 15ºC·min^{-1}, (b) 2ºC·min^{-1}, (c) 1ºC·min^{-1} and (d) 0.5ºC·min^{-1}. SAXD pattern (left) and SR-WAXD pattern (right). Inserted figure in (a) shows, in more detail, α (squares), β' (triangles) and β (diamonds) SR-WAXD peaks.

When the cooling rate was 15ºC·min^{-1}, we observed the crystallization of α at -51.1ºC, indicated by the long-spacing peak of 4.5nm and short-spacing peak of 0.431nm (Fig. 2). However, the more stable β'$_2$ form crystallized with the decreased cooling rates of 2, 1, and 0.5ºC·min^{-1}. The transformation pathways to more stable forms differed when starting from α or β'$_2$ crystals, although β phase was reached as the most stable form in both cases. The details of the experiment results are explained below.

After crystallization of α by cooling at 15ºC·min^{-1}, very complicated transformation processes occurred from α to β forms through intermediate forms during heating at 15ºC·min^{-1}, as demonstrated in a series of DSC endothermic and exothermic peaks (Fig. 1a) and changes in the SR-XRD WAXD patterns (Fig. 2a). First, melt-mediated transition occurred from α (melting at -34.1ºC) to β'$_2$ (crystallization at -32.3ºC). Although not detected in DSC peaks, transformation from β'$_2$ to β'$_1$ was observed at -20ºC, as indicated in the SR-XRD patterns (Fig. 2a). Another melt-mediated transformation then occurred from β'$_1$ (melting at -14.4ºC) to β (crystallization at -10.2ºC). Finally, β melted at -3.3ºC.

In the SR-XRD patterns, β'$_2$ form was identified by two new WAXD peaks with d-spacing values of 0.434nm and 0.405nm of β'$_2$, although the SAXD peak was maintained. On further

heating, a new peak at 0.393nm of β'_1 was detected in the WAXD pattern, corresponding to transformation from β'_2 to β'_1. However, no transition was observed in the DSC thermogram in the same temperature range. β'_1 melted at -14.4ºC (T_{onset}); soon after, β form crystallized at -10.2ºC (melt-mediated transition). This was confirmed by a shift from 4.5nm to 4.4nm in the SAXD pattern and by the most representative WAXD peaks with d-spacing values of 0.456nm, 0.448nm, 0.398nm, 0.389nm, and 0.376nm. This form finally melted at -3.3ºC (T_{onset}).

When the cooling rate was decreased to 2, 1, or 0.5ºC·min^{-1}, β'_2 form (instead of α was obtained from the melt, as indicated by the SAXD peak at 4.5nm and two WAXD peaks with d-spacing values of 0.434nm and 0.405nm (Figs. 2 b-d). The crystallization temperatures of β'_2 increased with decreasing cooling rates as follows: -26.6ºC at 2ºC·min^{-1}, -22.3ºC at 1ºC·min^{-1}, and -19.1ºC at 0.5ºC·min^{-1}. In these three cases, two onset temperatures were determined for the β'_2 crystallization peak (Table 2), as the complex DSC signal consisted of a main exothermic peak having a shoulder. Nevertheless, the beginning of the crystallization phenomenon corresponded to the first determined onset temperature. The transformation pathways from the starting polymorph β'_2 on heating were $\beta'_2 \rightarrow \beta'_1 \rightarrow$ liquid$\rightarrow\beta\rightarrow$liquid when the heating rate was 15ºC·min^{-1}. Transformation into β'_1 was indicated by XRD peaks at 0.452nm, 0.436nm, 0.407nm, and 0.393nm (WAXD pattern).

Even though the SR-XRD patterns exhibiting $\beta'_2 \rightarrow \beta'_1$ transformation on heating were quite similar to the three different cooling rates, the DSC patterns differed. When the cooling rate was 2ºC·min^{-1}, the $\beta'_2 \rightarrow \beta'_1$ transformation appeared as an exothermic DSC peak with an onset temperature of -20.8ºC. However, when the cooling rate was 1ºC·min^{-1}, this peak became endothermic (T_{onset}= -15.7ºC), and no peak was observed when the cooling rate was 0.5ºC·min^{-1}.

As no significant differences were detected in the SR-XRD patterns corresponding to the $\beta'_2 \rightarrow \beta'_1$ transformation in the three cases described above, no definitive explanation can be extracted from the different thermal behaviors observed. The variation of the cooling rate from 2 to 0.5ºC·min^{-1} may have influenced the subsequent $\beta'_2 \rightarrow \beta'_1$ transition, which occurred on the heating process. Probably, by varying the cooling rate, the crystallization process occurred through different mechanisms (e.g. the transformation from β'_2 to β'_1 may have partially occurred during cooling at 1 and 0.5ºC·min^{-1}, although not revealed by the SR-XRD data).

After the $\beta'_2 \rightarrow \beta'_1$ transition, melt-mediated transformation from β'_1 to β occurred on heating at a rate of 15ºC ·min^{-1}. The DSC patterns clearly exhibited endothermic peaks of β'_1 melting at -11 to -13ºC, which is associated with exothermic peaks of β crystallization at -6 to -4ºC (Fig. 1). Furthermore, β was easily identified by the shifting of the SAXD peak from 4.5nm to 4.4nm and the 0.458nm, 0.448nm, 0.398nm, 0.389nm, and 0.376nm WAXD peaks (Fig. 2). Finally, β form melted at 0.4ºC to 1.3ºC. The temperatures of melting of β'_1, crystallization, and melting of β somehow varied when the applied cooling rates changed from 2, 1, and 0.5ºC·min^{-1}. However, taking into account the error associated with the values given by the DSC data (see Table 2), we can assume that the temperatures at which each phenomenon occurred when different cooling rates were used are comparable.

It is noteworthy that the transformation characteristics from β'_2, which occurred after crystallization at the cooling rate of 2ºC·min^{-1}, changed when the heating rate was decreased from 15ºC·min^{-1} to 2ºC·min^{-1} (Fig. 3).

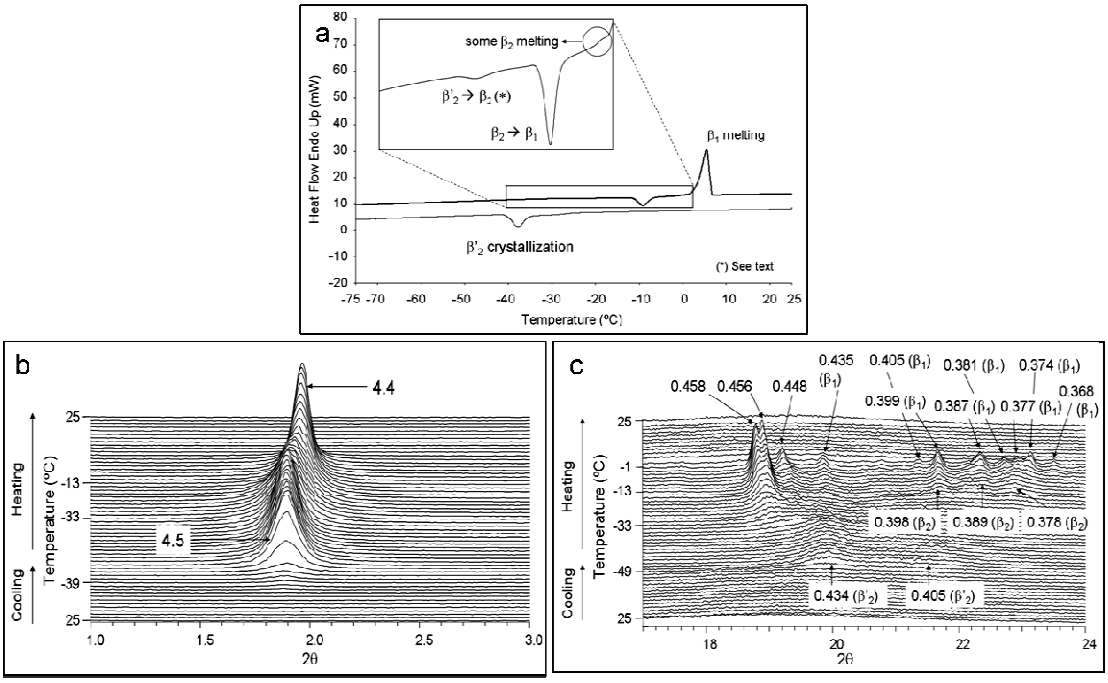

Figure 3. Polymorphic behavior of OOO when cooled at 2ºC·min^{-1} (β'_3 crystallization) and heated at 2ºC·min^{-1}. a) DSC thermogram. b) SR-SAXD pattern. c) SR-WAXD pattern.

Here, two β forms (β_2 and β_1) could be distinguished, as confirmed by the SR-XRD data and by the presence of a narrow melting peak with a shoulder at high temperatures in the DSC profile. Two consecutive transitions took place, from β'_2 to β_2 at T_{onset} of -25ºC and from β_2 to β_1 at T_{onset} of -11.3ºC (insert in Fig. 3a). It was difficult to clearly define the nature of the transformation pathway from β'_2 to β_2. However, the shape of the DSC peak indicated that the transition might occur through melt-mediated transformation with a broad and flat melting peak. At -33ºC, some changes could be observed in the SR-XRD WAXD pattern (e.g., decreased peak intensity), possibly due to some melting. Nevertheless, the only phenomenon that was easy to identify in the DSC profile was the exothermic peak with an onset temperature of -25ºC. We could easily detect the β_2 form through the WAXD peaks at 0.458nm, 0.398nm, 0.389nm, and

0.378nm. On further heating, another transformation (with T_{onset}= -11.3ºC) occurred to obtain another β form (β_1). Hence, we could distinguish between two β forms in OOO, as the typical WAXD peaks of β were maintained but a clear change was observed when new WAXD peaks of β_1 appeared at 0.381nm, 0.374nm, and 0.368nm. The melting curve of these two β forms appeared as a sharp melting peak (narrower than in the cases described above) with T_{onset} of 2.9ºC (due to β_1 melting) revealing a clear shoulder at -2.2ºC (β_2 melting). Therefore, as some β_2 melting was observed, we can conclude that not all β_2 transformed to β_1, as some melted at a higher temperature than that of the $\beta_2 \rightarrow \beta_1$ transformation. Comparison of the ΔH values associated with β melting when OOO was cooled at 2ºC·min^{-1} and heated at 15ºC·min^{-1} (melting ΔH of 73J·g^{-1}) and 2ºC·min^{-1} (melting ΔH of 128J·g-1) indicates an increase in the amount of β obtained as the heating rate was decreased.

Two β forms of OOO were previously indicated,[18] and the present study clearly confirmed it using SR-XRD data.

Micro-Raman experiments were carried out in order to study the polymorphic transformations that occurred when OOO was cooled and heated at 2ºC·min^{-1} (Fig. 4). Clear differences were observed in the spectra corresponding to the liquid state, β' and β forms. However, it was not possible to identify the two β forms.

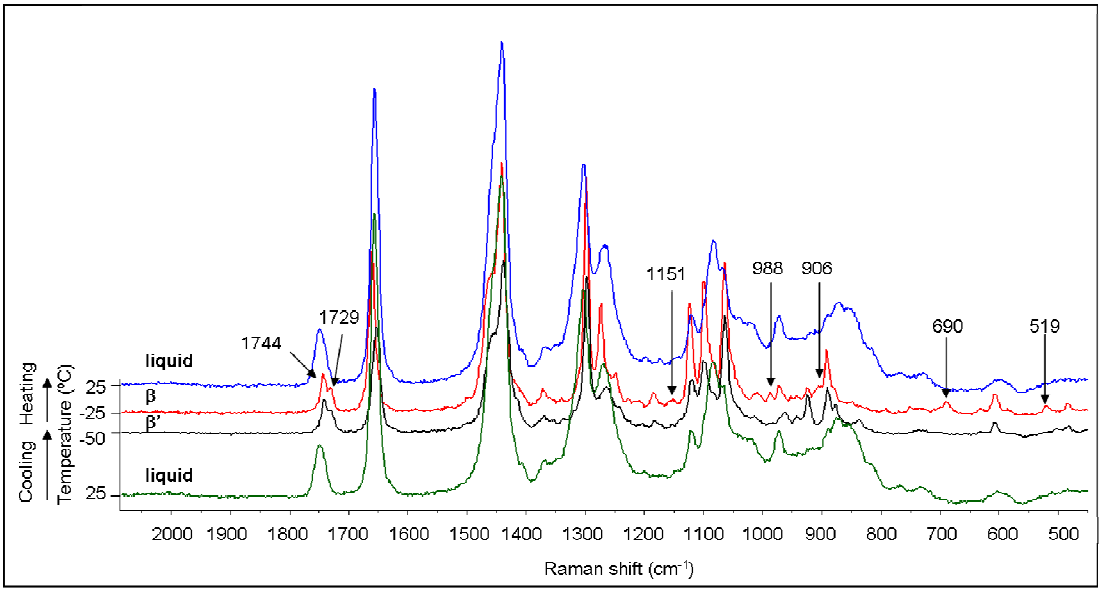

Figure 4. Raman spectra of OOO taken during cooling and heating processes at 2ºC·min^{-1}.

At -50ºC, β' form was detected; at -25ºC, it transformed to β form on heating. As Akita et al.[19] reported, the carbonyl stretch [ν(C = O)] band at 1749cm^{-1} in the liquid state split into two bands at 1744 and 1729cm^{-1} in β form. Subtle splitting could also be observed in the Raman spectrum corresponding to the β' form. According to Akita et al.,[19] the Raman C = C stretching band ν(C = C) is a good indicator of the conformation of the *cis*-olefin group. Thus, the band at 1653cm^{-1} in β' form shifted to 1660cm^{-1} in β form. Moreover, additional bands appeared at 1151, 988, 906, 690, and 519cm^{-1} when β' transformed to β form.

Figure 5 summarizes the polymorphic crystallization and transformation pathways of OOO.

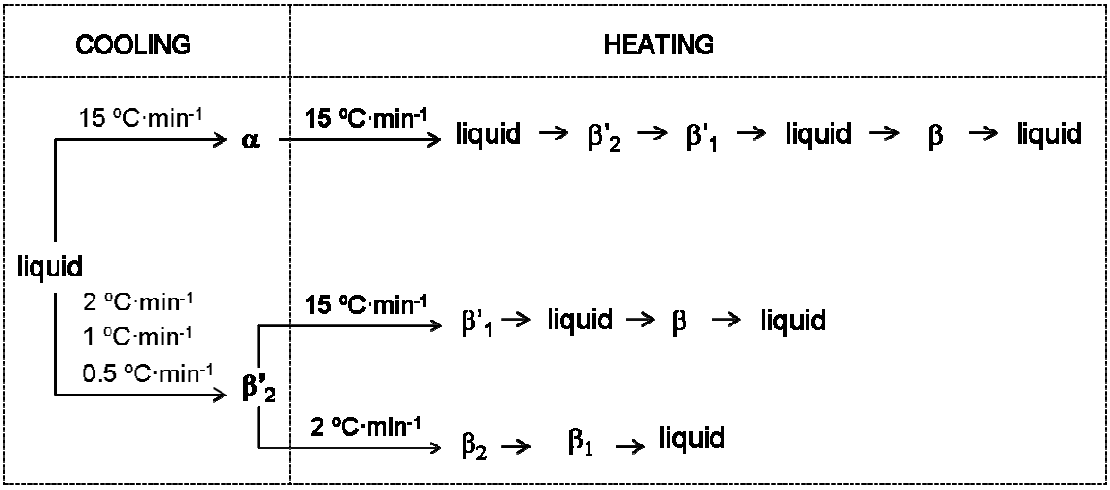

Figure 5. Polymorphic crystallization and transformation pathways of OOO under different cooling and heating conditions.

The α form was obtained by cooling OOO at 15ºC·min^{-1}. This α form did not exhibit the typical sharp WAXD peak of 0.41nm, corresponding to the hexagonal (H) subcell structure that appears in saturated, mono-, and diunsaturated TAGs.[7, 8] Here, the α form exhibited a broad peak at 0.431nm with a shoulder peak. This phenomenon has already been reported.[16, 19] For this result, Akita et al.[19] indicated an anisotropic lateral packing of hydrocarbon chains and a distorted H subcell structure. It was evident that the first-occurring polymorph changed from α to β'$_2$ with decreasing rates of cooling from 15ºC·min^{-1} to 2, 1, and 0.5ºC·min^{-1}. We have already observed the same results in OPO[7] and POP.[8]

Regarding the transformation pathways on heating, the polymorphic pathways depended mainly on heating rate and, as the Ostwald step rule predicts,[22] the first-occurring metastable forms were successively followed by other forms of increasing stability. Thus, the most stable β form was always reached at the two heating rates used (15 and 2ºC·min^{-1}) through β'$_2$ and β'$_1$.

Furthermore, when OOO was heated at the lower heating rate (2ºC·min^{-1}), it was possible to distinguish the two β forms (β_2 and β_1).

Polymorphic characteristics of OOL

OOL was also subjected to different thermal programs. Table 3 summarizes the melting temperatures and ΔH values when different rates of cooling (15, 2, and 0.5ºC·min^{-1}) and heating (15, 2 and 0.5º C·min^{-1}) were applied to the OOL samples. No β forms were present, and the most stable polymorph was β'. This result was the same as for 1,2-dipalmitoyl-3-myristoyl-*sn*-glycerol (PPM),[23] 1,2-dipalmitoyl-3-oleoyl-*rac*-glycerol (PPO),[24] 1,2-distearoyl-3-oleoyl-*rac*-glycerol (SSO),[25] 1-palmitoyl-2, 3-oleoyl-*rac*-glycerol (POO),[26] and 1-stearoyl-2, 3-oleoyl-*rac*-glycerol (SOO),[27] probably due to all these TAGs being asymmetric mixed-acid TAGs.

Table 3. DSC data of the polymorphic crystallization and transformation of OOLi obtained when the sample was cooled and heated at different rates. The letters *c*, *s* and *m* mean crystallization, solid-state transformation and melting, respectively. DSC onset temperatures were defined for crystallization and melting.

	Cooling (15ºC·min^{-1})	**Heating (15ºC·min^{-1})**			
Polymorph	α *(c)*	α *(m)*	β'_2 *(c)*	$\beta'_2 + \beta'_1$ *(m)*	
T_{onset} (ºC)	*	-65.5 ± 1.1	-57.8 ± 0.2	-25.4 ± 0.5	-24.0 ± 0.6
ΔH (J/g)		2 ± 1	-11 ± 2	72 ± 4**	
		(0.5ºC·min^{-1})			
Polymorph		$\alpha \rightarrow \beta'_2$	β'_1 *(m)*		
T_{onset} (ºC)		-65.2 ± 0.3	-20.9 ± 0.4		
ΔH (J/g)		-5 ± 2	79 ± 3		
	Cooling (2ºC·min^{-1})	**Heating (2ºC·min^{-1})**			
Polymorph	β'_1 *(c)*	β'_1 *(m)*			
T_{onset} (ºC)	-41.6 ± 0.4	-20.4 ± 0.8			
ΔH (J/g)	-61 ± 4	73 ± 3			
	Cooling (0.5ºC·min^{-1})	**Heating (15ºC·min^{-1})**			
Polymorph	β'_1 *(c)*	β'_1 *(m)*			
T_{onset} (ºC)	-33.4 ± 0.6	-21.9 ± 0.5			
ΔH (J/g)	-72 ± 4	80 ± 4			

* The α crystallization occurred during the isothermal and the beginning of the heating processes, so the DSC peak could not be interpreted as a function of temperature.

** These enthalpy values correspond to the global enthalpy of overlapped peaks.

The least stable polymorph (α was obtained when the cooling rate was high, whereas the most stable form (β'_1) crystallized from the melt at cooling rates of 2ºC·min^{-1} and 0.5ºC·min^{-1}. When the heating rate was varied, the most stable β'_1 form was obtained in all cases examined, similar to OOO.

Figure 6 depicts the polymorphic characteristics of OOL when it was cooled at a high rate (15ºC·min^{-1}) and heated at high (15ºC·min^{-1}) and low (0.5ºC·min^{-1}) rates.

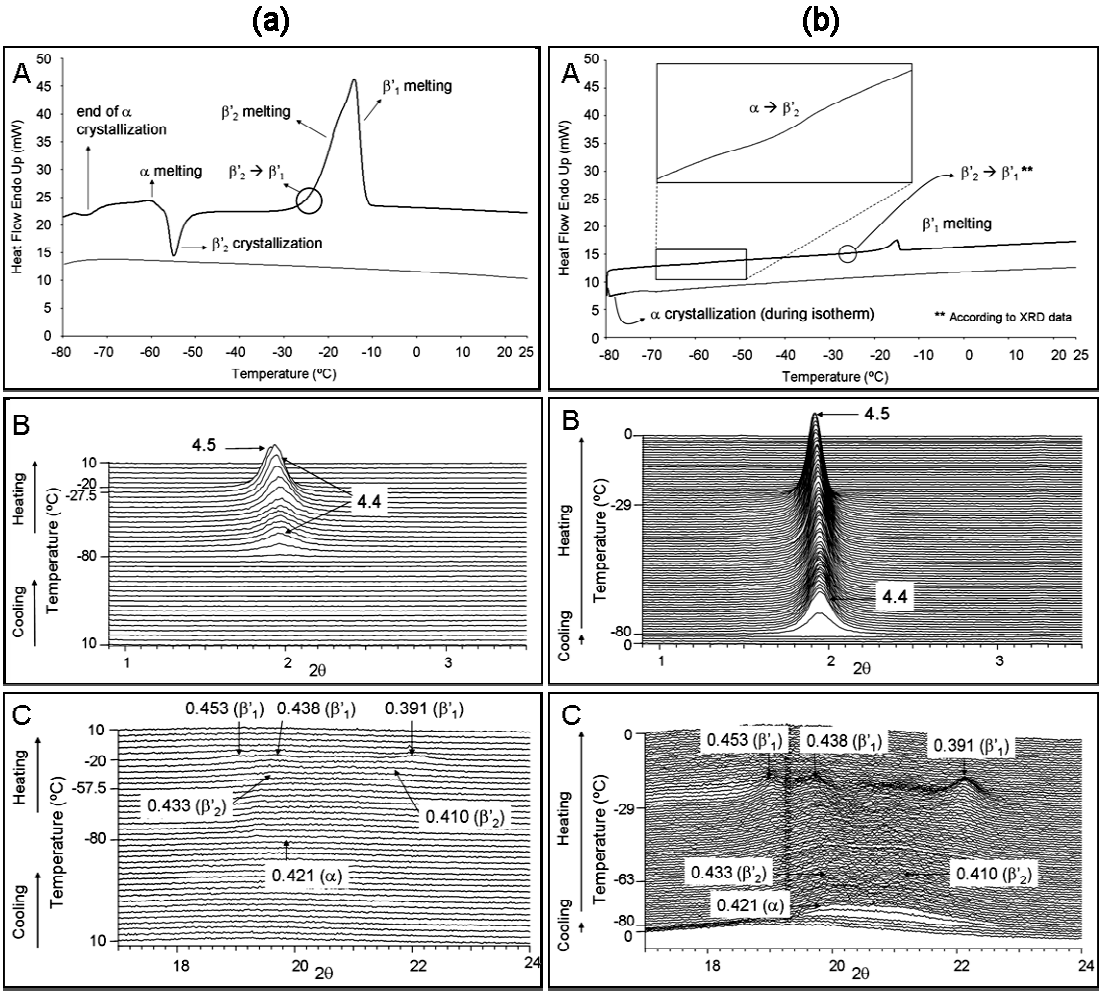

Figure 6. Polymorphic behavior of OOL (a) Cooling at 15ºC·min^{-1} and heating at 15ºC·min^{-1}. A. DSC thermogram. B. SR-SAXD pattern. C. SR-WAXD pattern. (b) Cooling at 15ºC·min^{-1} and heating at 0.5ºC·min^{-1}. A. DSC thermogram. B. SR-SAXD pattern. C. SR-WAXD pattern.

At 15ºC·min^{-1}, the α form, □with a long-spacing of 4.4nm and a single short-spacing of 0.421nm, crystallized. Similar to OOO, the broad WAXD peak at 0.421nm had a shoulder. No exothermic DSC peak corresponding to this crystallization was observed in the cooling thermal step, due to the low crystallization temperature of this polymorphic form and the high cooling rate used. The α crystallization started during the isotherm (1min long) that took place between the cooling and heating steps, and ended at the beginning of the heating process (Fig. 6(a)A).

After α crystallization, melt-mediated transformation from α to β'$_2$ occurred when the sample was heated at 15ºC·min^{-1}, as observed in the melting of α at -65.5ºC and the crystallization of β'$_2$ at -57.8ºC, (Fig. 6(a)A). This was clearly demonstrated by the presence of the β'$_2$ WAXD broad peaks at 0.433nm and 0.410nm (Fig. 6(a)B). Later, the SR-XRD data indicated that β'$_2$ transformed to β'$_1$ before β'$_1$ melted. During this transformation, the SAXD peak shifted from 4.4nm to 4.5nm, and new WAXD peaks of β'$_1$ appeared at 0.453nm, 0.438nm, and 0.391nm. Apparently not all β'$_2$ transformed to β'$_1$, as the last melting peak seemed to be double, with clear onset temperatures of -25.4ºC (corresponding to β'$_2$ melting) and -24ºC (corresponding to β'$_1$ melting).

Solid-state α→β'$_2$ transformation occurred at a heating rate of 0.5ºC·min^{-1}, as indicated by an exothermic DSC peak (insert in Fig. 6(b)A). This contrasts with the melt-mediated α→β'$_2$ transformation obtained by heating at 15ºC·min^{-1}. This solid-state transformation occurred at -65.2ºC; concurrently, β'$_2$ WAXD peaks of 0.433nm and 0.410nm appeared. Later, β'$_2$→β'$_1$ transformation occurred at -39ºC, as indicated by the SAXD peak shifting from 4.4nm to 4.5nm and WAXD peaks at 0.453nm, 0.438nm, and 0.391nm, although no DSC thermopeaks were

observed. The β'_1 form finally melted at -20.9ºC. As explained above, not all β'_2 transformed to β'_1 at the heating rate of 15ºC·min^{-1}, as β'_2 melting was observed together with the melting of β'_1. Not surprisingly, β'_2 had enough time to transform completely to β'_1, and β'_1 melted afterwards at a lower heating rate of 0.5ºC·min^{-1}.

The effects of the decreased cooling rate on the polymorphic crystallization of OOL were clearly observed. Figure 7 depicts the DSC and laboratory-scale XRD data of OOL when it was cooled and heated at 2ºC·min^{-1}.

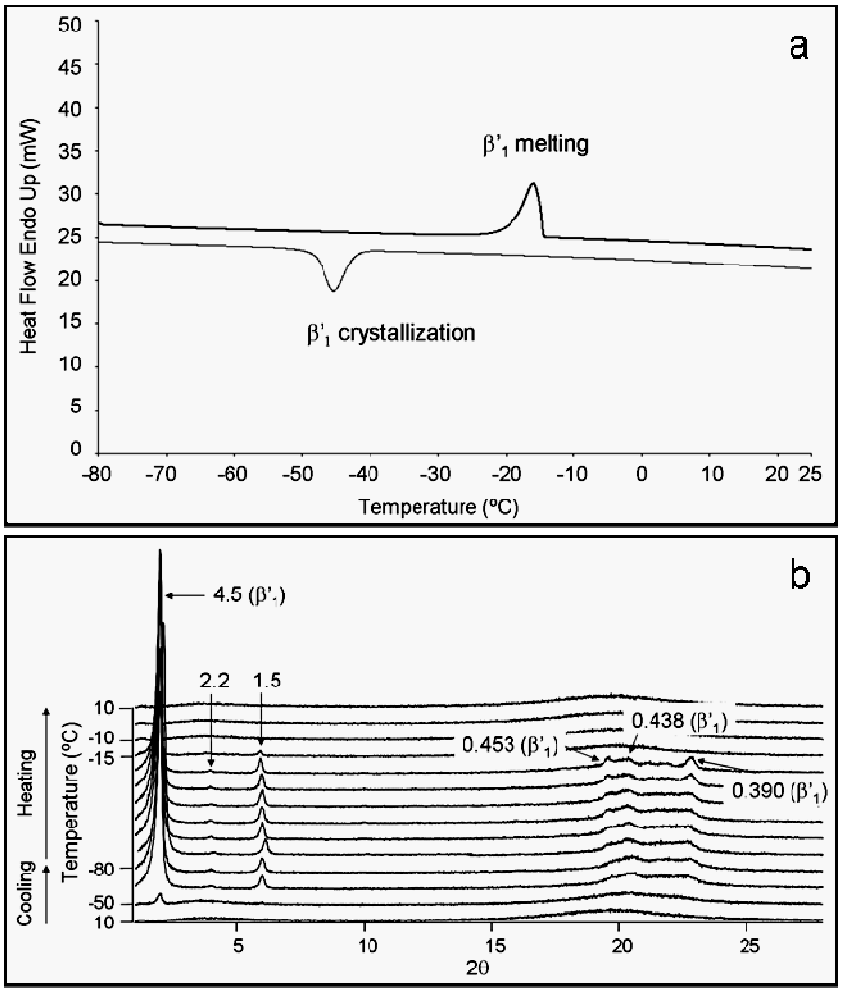

Figure 7. Polymorphic behavior of OOL when cooled at 2ºC·min^{-1} (β'$_1$ crystallization) and heated at 2ºC·min^{-1}. a) DSC thermogram. b) Laboratory-scale XRD pattern.

Figure 8 presents the results obtained for cooling at 0.5ºC·min^{-1} and heating at 15ºC·min^{-1}.

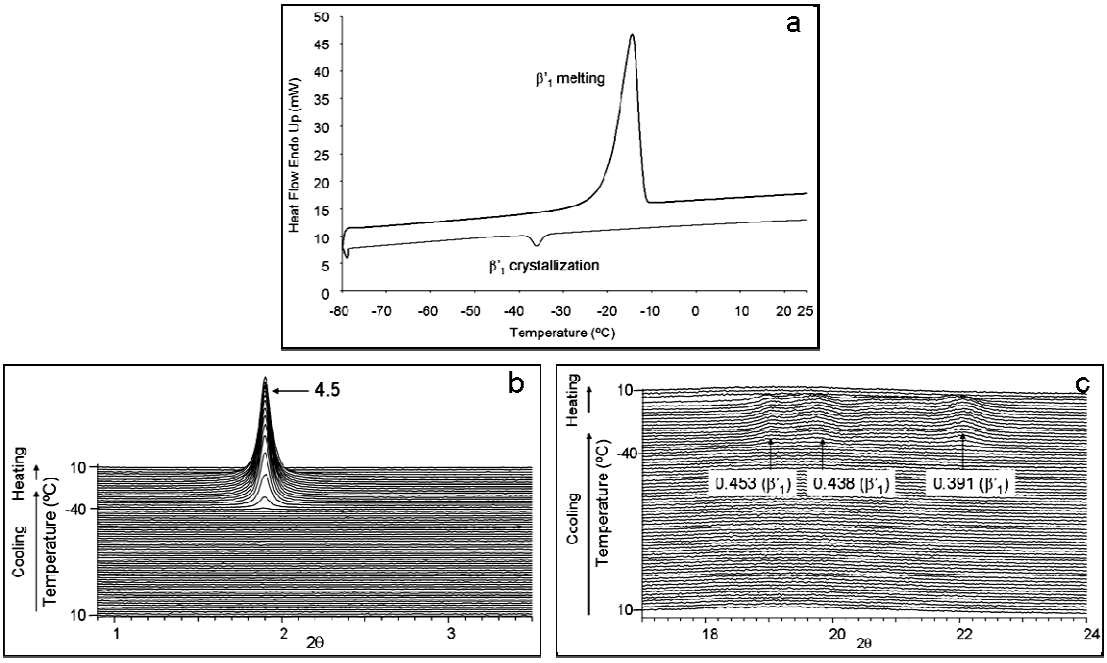

Figure 8. Polymorphic behavior of OOO when cooled at 0.5ºC·min^{-1} (β'$_1$ crystallization) and heated at 15ºC·min^{-1}. a) DSC thermogram. b) SR-SAXD pattern. c) SR-WAXD pattern.

When lower cooling rates were applied (2 and 0.5ºC·min^{-1}), the first-occurring form was the most stable β'$_1$. The crystallization temperatures of β'$_1$ were -41.6ºC for cooling at 2ºC·min^{-1} and -33.4ºC for cooling at 0.5ºC·min^{-1}. In both cases, the typical XRD peaks of β'$_1$ were observed, and no β'$_2$ form was present.

When β'$_1$ crystals were heated, they simply melted at -21 to -20ºC without transformation to β form.

Figure 9 summarizes the polymorphic characteristics of OOL observed by varying the cooling and heating rates.

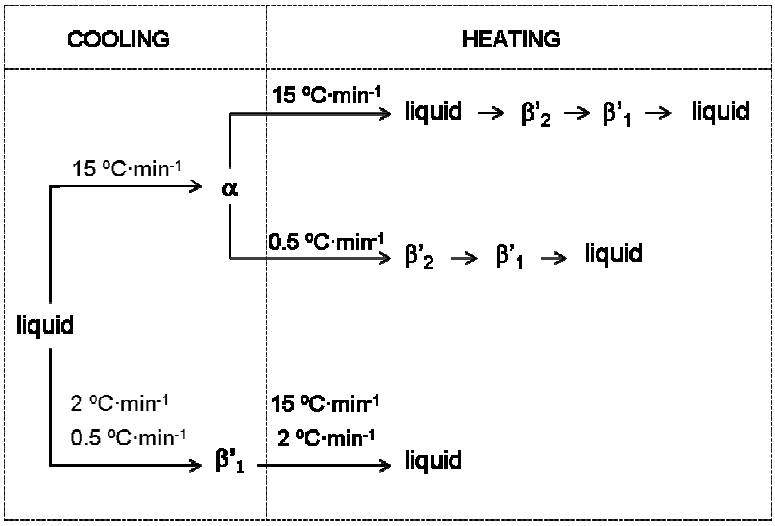

Figure 9. Polymorphic crystallization and transformation pathways of OOL under different cooling and heating conditions.

High cooling rates caused the crystallization of α (least stable form), while intermediate and low cooling rates led to the crystallization of the most stable β'_1 form. Starting from α crystals, the sequence of polymorphs of increasing stability when the heating rate was high (15ºC·min^{-1}) was α→liquid→β'_2→β'_1→liquid; however, when the heating rate was low (0.5ºC·min^{-1}), it changed to α→β'_2→β'_1→ liquid. The difference between the two pathways was apparent in the nature of the α→β'_2 transition: melt-mediation at 15ºC·min^{-1} and solid-state at 0.5ºC·min^{-1}. This was quite similar to that observed for 1,3-dipalmitoyl-2-oleoyl glycerol (POP).[8]

The present study has demonstrated the following kinetic properties of polymorphic crystallization and transformation of OOO and OOL, which were affected by different thermal treatments.

(1) Five polymorphs (α, β'_2, β'_1, β_2, and β_1) were isolated in OOO, and three polymorphs (α,β'_2 and β'_1) in OOL.

(2) The effects of varying cooling and heating rates were remarkable. More stable polymorphs were crystallized by decreasing the cooling rates, whereas less stable polymorphs were manifest at higher cooling rates.

(3) Solid-state transformations occurred more easily than melt-mediated transformation when the heating rate was decreased.

These properties were consistent with those observed for POP and OPO, whose crystallization and transformation properties were examined with DSC and SR-XRD at cooling and heating rates of 15ºC·min^{-1} to 0.5ºC·min^{-1} (Table 4).

Table 4. Crystallization and transformation pathways of POP, OPO, OOO and OOL at different cooling and heating rates, in which *mm* and *ss* mean melt-mediated and solid-state transformations.

		POP	OPO	OOO	OOL
Polymorphs		α–2, γ–3, β'–2[a], δ–3, β–3 [a]	α–2, β'–2[a] , β–3	α–2, β'–2[a] , β–2 [a]	α–2, β'–2[a]
Crystallization on cooling	rapid	α	α	α	α
	slow	γ	β' + β	β'	β'
Transformation	rapid	α→(*mm*)β'→L	α→(*mm*) β'→β→L	α→(*mm*) β'→(*mm*) β→L	α→(*mm*) β'→L

on heating		γ→L	β'→β→L	β'→(*mm*) β→L	β'→L
	slow	α→γ→(ss)δ→(*mm*) β→L	n.a[b]	n.a[b]	α→(*ss*) β'→L
		γ→(*mm*) β'+δ→(*mm*) β→L	n.a[b]	β'→(*ss*) β→L	β'→L

[a] For simplicity, β_2' and β_1' or β_2 and β_1 are summarized into β' or β, respectively.

[b] Not available.

For OPO, multiple polymorphic forms involving the most stable β form were obtained, demonstrating complex concurrent crystalization in most cases. For POP, however, it was dificult to obtain stable forms such as β' and β even when the cooling rate was lowered to 0.5ºC·min^{-1}; for example, γ was obtained instead of β' form. In the present study, for OOO and OOL, α was crystallized with rapid cooling, and β' was crystallized with slow cooling.

More stable forms (e.g., β' and β were obtained either through solid-state or melt-mediated transformation for OPO, OOO, and OOL even at a high rate (15ºC·min^{-1}). However, it was necessary to decrease the heating rates to 2 to 0.1ºC·min^{-1} to obtain the most stable β form for POP. Thus, we may conclude that similar characteristics of polymorphic crystallization and transformation were observed for OPO, OOO, and OOL; however, POP differed in the difficulty of obtaining the most stable β form.

We may explain these results by taking into account the activation energies of solid-state and melt-mediated transformations from one polymorphic form to another, as fully discussed for POP.[8] Figure 10 illustrates two typical transformations that take place from a less stable form (A) to a more stable form (B). The rates of transformation are basically determined by the magnitude of the activation free energies ($\Delta G^{\#}$) involved in each process: the larger the $\Delta G^{\#}$, the lower the transformation rate.

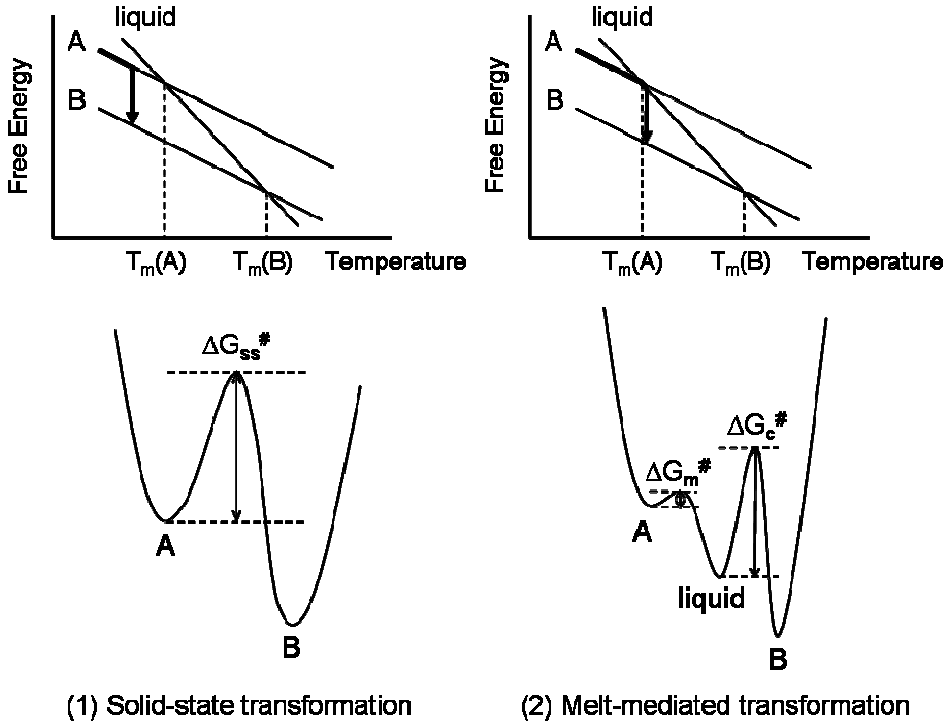

Figure 10. Activation free energy ($\Delta G^{\#}$) for solid-state and melt-mediated transformation from metastable A to more stable B forms.

As for solid-state transformation, $\Delta G_{ss}^{\#}$ may include excess energy to enable structural changes (e.g., subcell structure and chain-length structure) needed to cause transformation from form A to form B. The rate of the melt-mediated transformation is determined by the magnitude of $\Delta G_m^{\#}$ corresponding to the melting of form A and the subsequent crystallization ($\Delta G_c^{\#}$) of form B.

However, the actual rate may be determined by $\Delta G_c^{\#}$ because of the ease of melting and the small values of $\Delta G_m^{\#}$.

We may simply assume that the values of $\Delta G_{ss}^{\#}$ for transformations involving change from loosely packed subcell structures (e.g., hexagonal (α polymorph)) to more closely packed subcell structures of $O_{\perp}$ (β') and $T_{//}$ (β) are larger than those from $O_{\perp}$ (β') to $T_{//}$ (β). Also the values of $\Delta G_{ss}^{\#}$ may be lower for transformation between polymorphs having the same double chain length structures than for changes from double to triple chain length structures (Fig. 11).

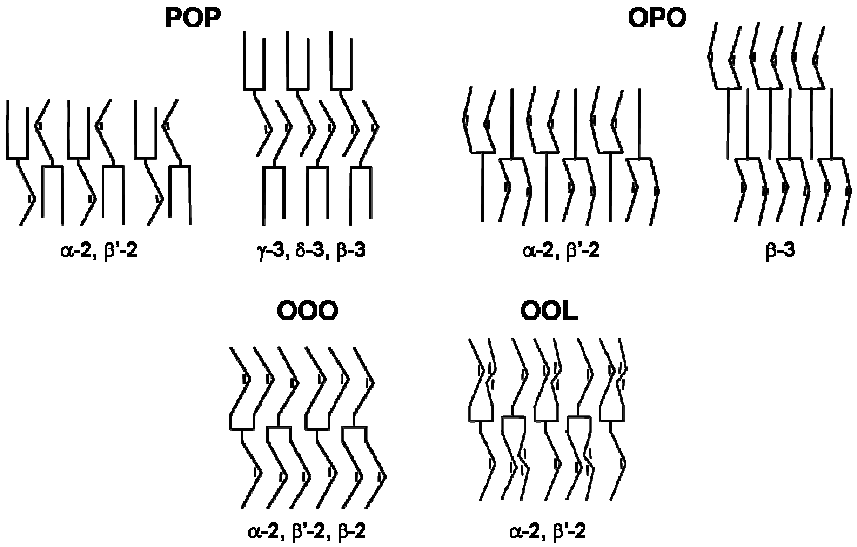

Figure 11. Structure models of POP, OPO, OOO and OOL. For simplicity, multiple β' and β forms are represented by β' and β.

The same assumption may apply to crystallization, in that the values of $\Delta G_c^{\#}$ of the polymorphs having tightly packed subcell and triple chain length structures may be larger than in the other

cases. Taking into account these points, the crystallization and transformation of more stable β and β' forms of OOO and OOL occur easily, since the all polymorphic forms exhibit the same double chain length structure.

A peculiarity in the transformation pathways was observed for POP in that, even during slow heating, solid-state transformation occurred with more difficulty, compared to the OOO and OOL cases. This may be due to the fact that POP contains saturated fatty acid (palmitic acid) moiety whose transformation from less stable to more stable forms may need large activation energies ($\Delta G_{ss}^{\#}$) compared with those of oleic and linoleic acid moieties. The flexibility of the chain packing of unsaturated acids is more enhanced than that of saturated fatty acids.[28] This may decrease the value of $\Delta G_{ss}^{\#}$ for transformation into more stable forms of OOO and OOL.

To conclude, the present study has found that the occurrence and transformation processes of metastable and more stable polymorphs of OOO and OOL were drastically modified by changing the rates of cooling as well as heating. It may be worth to note that such effects were recently observed in molecular crystals using an ultrafast DSC technique.[29]

AUTHOR INFORMATION

Corresponding Author

Phone: +34 93 402 13 50. Fax: +34 93 402 13 40. E-mail: laurabayes@ub.edu

ACKNOWLEDGMENT

The authors acknowledge the financial support of the Ministerio de Economía y Competitividad through Project MAT2011-27225, the Generalitat de Catalunya through the Grup Consolidat (SGR 2009 1307), and the Ministerio de Educación through the Factoría Cristalográfica (Consolider-Ingenio CSD2006-15) and through the Beca del Programa de Formación de Profesorado Universitario (FPU). SR-XRD experiments were conducted with the approval of the Photon Factory Program Advisory Committee (proposals 2010G114 and 2010G656). The authors gratefully acknowledge the help of Prof. Masaharu Nomura, Station Manager of BL-9C and Associate Prof. Noriyuki Igarashi, Station Manager of BL-15A at Photon Factory.

REFERENCES

1. Lipids: Structure, Physical Properties and Functionality; Larsson, K., Quinn, P., Sato, K., Tiberg, F., Eds.; The Oily Press: Bridgwater, England, 2006.

2. Physical Properties of Lipids; Marangoni, A. G., Narine, S.S., Eds.; Marcel Dekker: New York, USA, 2002, 63-217.

3. Smith, K. W.; Bhaggan, K.; Talbot, G.; van Malssen, K. F. Crystallization of Fats: Influence of Minor Components and Additives. *J. Am. Oil Chem. Soc.* **2011**, 88, 1085-1101.

4. Mazzanti, G.; Li, M.; Marangoni, A. G.; Idziak, S. H. J. Effects of Shear Rate Variation on the Nanostructure of Crystallizing Triglycerides. *Cryst. Growth Des.* **2011**, 11, 4544-4550.

5. Ueno, S.; Ristic, R. I.; Higaki, K.; Sato, K. *In situ* Studies of Ultrasound-Stimulated Fat Crystallization Using Synchrotron Radiation. *J. Phys. Chem. B.* **2003**, 107, 4927-4935.

6. Rousset, P.; Rappaz, M.; Minner, E. Polymorphism and Solidification Kinetics of the Binary System POS-SOS. *J. Am. Oil Chem. Soc.* **1998**, 75, 857-864.

7. Bayés-García, L.; Calvet, T.; Cuevas-Diarte, M. A.; Ueno, S.; Sato, K. *In situ* synchrotron radiation X-ray diffraction study of crystallization kinetics of polymorphs of 1,3-dioleoyl-2-palmitoyl glycerol (OPO). *CrystEngComm.* **2011**, 13, 3592-3599.

8. Bayés-García, L.; Calvet, T.; Cuevas-Diarte, M. A.; Ueno, S.; Sato, K. *In situ* observation of transformation pathways of polymorphic forms of 1,3-dipalmitoyl-2-oleoyl glycerol (POP) examined with synchrotron radiation X-ray diffraction and DSC. *CrystEngComm*. **2013**, 15, 302-314.

9. Foubert, I.; Fredrick, E.; Vereecken, J.; Sichien, M.; Dewettinck, K. Stop-and-return DSC method to study fat crystallization. *Thermochim. Acta.* **2008**, 471, 7-13.

10. Campos, R.; Narine, S. S.; Marangoni, A. G. Effect of cooling rate on the structure and mechanical properties of milk fat and lard. *Food Res. Int.* **2002**, 35, 971-981.

11. Svenstrup, G.; Bruggemann, D.; Kristensen, L.; Risbo, J.; Skibsted, L. H. The influence of pretreatment on pork fat crystallization. *Eur. J. Lipid Sci. Technol.* **2005**, 107, 607-615.

12. Campos, R.; Ollivon, M.; Marangoni, A. G. Molecular Composition Dynamics and Structure of Cocoa Butter. *Cryst. Growth Des.* **2010**, 10, 205-217.

13. Chiavaro, E.; Rodríguez-Estrada, M. T.; Bendini, A.; Cerretani, L. Correlation between thermal properties and chemical composition of Italian virgin olive oils, *Eur. J. Lipid Sci. Technol.* **2010**, 112, 580-592.

14. Timms, R. E. Fractional crystallization-the fat modification process for the 21st century. *Eur. J. Lipid Sci. Technol.* **2005**, 107, 48-57.

15. Wheeler, D. H.; Riemenschneider, R. W.; Sando, C. E. Preparation, Properties and Thiocyanogen Absortion of Triolein and Trilinolein. *J. Biol. Chem.* **1940**, 132, 687-699.

16. Ferguson, R. H.; Lutton, E. S. The Polymorphism of Triolein. *J. Am. Chem. Soc.* **1947**, 69, 1445-1449.

17. Hagemann, J. W.; Tallent, W. H.; Kolb, K. E. Differential Scanning Calorimetry of Single Acid Triglycerides: Effect of Chain Length and Unsaturation. *J. Am. Oil Chem. Soc.* **1972**, 49 (2), 118-123.

18. Sato, K.; Ueno, S. in Bailey's Industrial Oil and Fat Products, ed. Shahidi, F. John Wiley & Sons Inc., Hoboken, New Jersey, USA, 2005, vol. 1, pp. 77–120.

19. Akita, A.; Kawaguchi, T.; Kaneko, F. Structural Study on Polymorphism of Cis-Unsaturated Triacylglycerol: Triolein. *J. Phys. Chem. B.* **2006**, 110, 4346-4353.

20. Mortimer, R. G. Mathematics for Physical Chemistry; Elsevier Academic Press: San Diego, USA, 2005, 326.

21. Chapman, D. The Polymorphism of Glycerides. *Chem. Rev.* **1962**, 62(5), 433-456.

22. Ostwald, W. Studien über die Bildung und Umwandlung fester Körper. *Z. Phys. Chem.* **1897**, 22, 289-330.

23. Kodali, D. R., Atkinson, D., Small, D. M. Polymorphic behavior of 1,2-dipalmitoyl-3-lauroyl(PP12)- and 3-myristoyl(PP14)-*sn*-glycerols. *J. Lipid Res.* **1990**, 31, 1853-1864.

24. Minato, A.; Ueno, S.; Smith, K.; Amemiya, Y.; Sato, K. Thermodynamic and Kinetic Study on Phase Behavior of Binary Mixtures of POP and PPO Forming Molecular Compound Systems. *J. Phys. Chem. B* **1997**, 101, 3498-3505.

25. Takeuchi, M.; Ueno, S.; Sato, K. Crystallization kinetics of polymorphic forms of a molecular compound constructed by SOS (1,3-distearoyl-2-oleoyl-*sn*-glycerol) and SSO (1,2-distearoyl-3-oleoyl-*rac*-glycerol). *Food Res. Int.* **2002**, 35, 919-926.

26. Zhang, L.; Ueno, S.; Miura, S.; Sato, K. Binary Phase Behavior of 1,3-Dipalmitoyl-2-oleoyl-*sn*-glycerol and 1,2-Dioleoyl-3-palmitoyl-*rac*-glycerol. *J. Amer. Oil Chem. Soc.* **2007**, 84, 219-227.

27. Zhang, L.; Ueno, S.; Sato, K.; Adlof, R. O.; List, G. R. Thermal and structural properties of binary mixtures of 1,3-distearoyl-2-oleoyl-glycerol (SOS) and 1,2-dioleoyl-3-stearoyl-*sn*-glycerol (*sn*-OOS). *J. Therm. Anal. Calorim.*, **2009**, 98, 105-111.

28. Small, D. M. Lateral chain packing in lipids and membranes. *J. Lipid Res.*, **1984**, 25, 1490-1500.

29. Jiang, J.; Zhuralev, E.; Huang, Z.; Wei, L.; Shan, M.; Xue, G.; Zhou, D.; Schick, C.; Jian, W. A transient polymorph transition of 4-cyano-4'-octyloxybiphenyl (8CB) revealed by ultrafast differential scanning calorimetry (UFDSC). *Soft Matter*, **2013**, 9, 1488-1491.

TABLE OF CONTENTS IMAGE

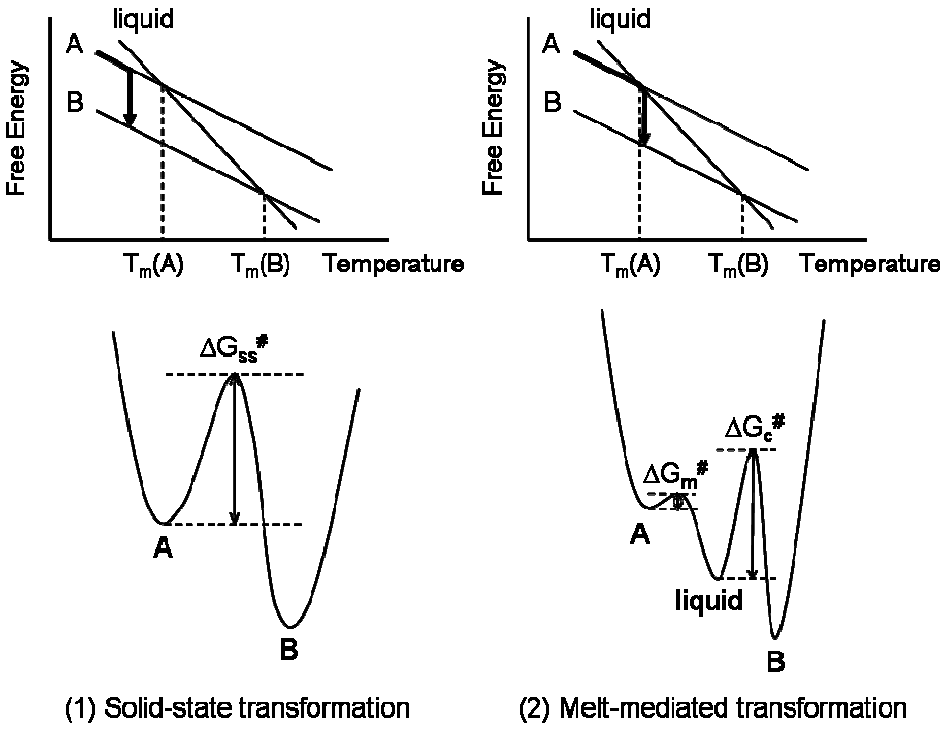

(1) Solid-state transformation (2) Melt-mediated transformation